Applied Catalysis B: Environmental 142–143 (2013) 323–328

Contents lists available at SciVerse ScienceDirect

Applied Catalysis B: Environmental

journal homepage: www.elsevier.com/locate/apcatb

Facile fabrication of platinum nanobubbles having efficient catalytic degradation performances

Jin-Ah Kwak, Dong Ki Lee, Du-Jeon Jang*

School of Chemistry, Seoul National University, NS60, Seoul 151-742, Republic of Korea

ARTICLE INFO

Article history:
Received 8 March 2013
Received in revised form 19 April 2013
Accepted 20 May 2013
Available online 28 May 2013

Keywords:
Catalysis
Degradation
Rhodamine B
Core–shell nanocomposite
Nanoshell

ABSTRACT

Platinum nanobubbles having a uniform shell thickness of 20 nm with average outer diameters of 150, 320, and 420 nm have been synthesized readily by etching the silica cores of SiO_2@Pt core–shell nanospheres and they have been found to catalyze the degradation of rhodamine B efficiently in the presence of KBH_4 compared with SiO_2@Pt core–shell nanospheres. The catalytic rate constant of the nanobubbles ($0.030\ min^{-1}$) with an activation energy of 10.7 kcal mol^{-1} is larger by 23 times than that of the core–shell nanospheres with an activation energy of 30.5 kcal mol^{-1}. The catalytic activation energy and the entropy of activation obtained from the Arrhenius and the Eyring plots, respectively, have been found to increase with the size increase of platinum nanobubbles, due to the reduction of the nanoreactor confinement effect of platinum nanobubbles. The existence of a good compensation effect between activation energies and frequency factors has been evidenced to support that the catalytic degradation reaction takes place within the nanocavities of platinum nanocatalysts.

1. Introduction

The controlled fabrication, characterization, and application of nanometer-sized materials with functional properties have been studied widely [1–5]. In particular, noble-metal nanostructures with different sizes and shapes have been studied extensively, because they can be possibly used in diverse applications such as catalysts, devices, transistors, and optoelectronics [6,7]. Various properties of noble-metal nanostructures, which are very different from those of bulk materials, can be changed by controlling sizes and shapes, because their unusual properties arise from their large surface area-to-volume ratio and the spatial confinement of electrons, phonons, and electric fields in and around them [8]. Noble-metal nanoparticles show strong UV/vis absorption bands depending on sizes and shapes due to the collective excitations of electrons in the conduction band, known as localized surface plasmon resonances [9–13]. Among various noble-metal nanostructures, platinum-based nanostructures especially have attracted widespread interest as platinum plays an outstanding role in multifunctional catalysts for many industrial reactions [14,15]. However, because there are some crucial obstacles such as low platinum-utilization efficiency and high cost, some ways must be found to reduce the amount of platinum used in specific applications by increasing its catalytic activity in order to lower the overall cost [16]. Thus, it is necessary to thoroughly understand the behaviors of platinum nanoparticles in nanocatalysis. The waste water produced in textile and dye industry has a very bad effect on the environment, due to their large discharge volume and toxic composition. With the development of dye industry, the studies on the treatment of waste water containing dyestuffs have become increasingly important [17]. The decomposition of these organic pollutants via catalytic oxidation or reduction using nanocatalysts is considered to be the most efficient green method for the management of organic wastes [18]. Treatment with strong reducing agents such as KBH_4 can reduce color in dye effluents such as rhodamine B. The reducing compounds chemically break the double bonds of azo dyes and produce aromatic amines of lower molecular weight [19].

Various strategies have been developed to improve the performance of platinum catalysts. In particular, the reactivity of platinum nanocatalysts depends highly on their structures, so many researchers have studied the morphology of platinum nanostructures and have synthesized diverse nanostructures of platinum. For example, El-Sayed et al. have compared the stability and catalytic activities of tetrahedral, spherical, and cubic platinum nanoparticles with different sizes for the electron-transfer reaction between hexacyanoferate ions and thiosulfate ions. The catalytic activity of nearly spherical nanoparticles has been reported to be intermediate between those of tetrahedral and cubic nanoparticles [20,21]. Considerable studies have been focused

* Corresponding author. Tel.: +82 2 880 4368; fax: +82 2 875 6624.
E-mail address: djjang@snu.ac.kr (D.-J. Jang).

0926-3373/$ – see front matter © 2013 Elsevier B.V. All rights reserved.
http://dx.doi.org/10.1016/j.apcatb.2013.05.037

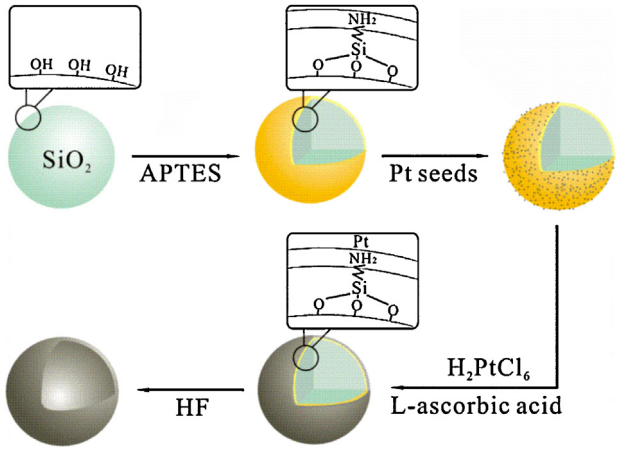

Fig. 1. Schematic for the fabrication of platinum nanobubbles.

on the syntheses of variously shape-controlled platinum nanostructures such as nanospheres, nanorods, nanowires, nanotubes, and nanodendrites [22–26]. Especially, hollow-structured platinum nanoparticles can be applied to nanometer-sized chemical reactors, efficient catalysts, and energy-storage media, and small containers to encapsulate multi-functional active materials, and they have structurally tunable features such as thickness, interior cavity size, and chemical composition [27,28]. In general, the syntheses of hollow nanostructures have been based on specific theories like the Kirkendall effect, the Ostward ripening, and the layer-by-layer assembly, and they can be divided into four categories: conventional hard-templating, sacrificial-templating, soft-templating, and template-free methods [29–32].

Herein, we demonstrate a facile and efficient method to synthesize platinum-based nanocatalysts having nanobubble structures using a conventional hard template (Fig. 1). The preparation of hollow structures by using against a hard material as templates is conceptually straightforward, and it involves four major steps: the preparation of hard templates, the functionalization/modification of template surfaces to achieve favorable surface properties, the coating of the templates with designed materials or their precursors, possibly with post treatment to form compact shells, and the selective removal of the templates to obtain hollow structures. We have used monodispersive silica nanospheres as hard templates. These templates are advantageous for diverse reasons including their narrow size distribution, availability in relatively large amounts and in a wide range of sizes from commercial sources, and simplicity of their synthesis using well-known formulations. Next, templates were functionalized with amino groups and coated with platinum seeds. Finally, platinum nanobubbles were made by etching the silica nanocores of SiO_2@Pt core–shell nanospheres with HF(aq). The produced nanobubbles have been found to catalyze the degradation of rhodamine B efficiently with a remarkably reduced activation energy in the presence of KBH_4 compared with SiO_2@Pt core–shell nanospheres.

2. Experimental

2.1. Materials

H_2PtCl_6 (s, 99.995%), tetraethyl orthosilane (ℓ, TEOS, ≥99%), L-ascorbic acid(s), 25% NH_3(aq), (3-aminopropyl)triethylsilane (ℓ, APTES, 98%), 50% HF(aq), 35% HCl(aq), polyvinylpyrrolidone (s, PVP, M.W. = 25000), $NaBH_4$ (s, 99.995%), rhodamine B (s), KBH_4 (s, ≥95%), and ethanol (ℓ) were used as purchased from Sigma–Aldrich. Ultrapure deionized water (>17 MΩ cm) was obtained using a Millipore Milli-Q system.

2.2. Preparation of platinum nanocatalysts

All the synthetic processes of platinum nanocatalysts were taken place under ambient conditions. Monodispersive silica nanospheres were prepared from the sol-gel process of TEOS under base catalysis following the Stöber method [33]. 25.00 mL of ethanol, 4.50 mL of H_2O, 1.55 mL of TEOS, and a specified volume of 25% NH_3(aq) were mixed and kept under vigorous stirring for 1 h. 0.40, 0.96, and 1.92 mL of 25% NH_3(aq) were used to synthesize silica nanospheres, which were used later to fabricate platinum nanobubbles of 150, 250, and 400 nm, respectively, in an average outer diameter [34]. Produced silica nanospheres were centrifuged at 10,000 rpm for 10 min and redispersed in 31.45, 32.01, and 32.97 mL, respectively, of ethanol three times.

Platinum seeds were prepared by reducing H_2PtCl_6 in an aqueous PVP solution. 10.0 mg of H_2PtCl_6(s) was dissolved in 10.00 mL of 35% HCl(aq), the solution was mixed with 10.00 mL of 2.0 M $NaBH_4$(aq) and 10.00 mL of 0.3 g L^{-1} PVP(aq) at once, and the solution was not stirred during the reaction [35]. The products were centrifuged at 10,000 rpm for 10 min and redispersed in 30.00 mL of ethanol three times.

For the modification of the surfaces of silica nanospheres with amino groups, 10.00 mL of silica nanospheres-dispersed ethanol was mixed with 5.00 mL of 1.0 M APTES in ethanol and kept under vigorous stirring for 2 h.

5.00 mL of platinum seeds was added to the above mixture solution and stirred for 1 h to attach platinum seeds on the surfaces of APTES-treated silica nanospheres. For the transformation of platinum seeds into platinum shells, 4.00 mL of 2 days-aged 10 mM H_2PtCl_6(aq) and 2.00 mL of the above mixture solution were mixed and stirred for 1 h. Then, 0.32 mL of 100 mM L-ascorbic acid(aq) was added and the reaction mixture was stirred for 1 h. Note that the molar concentration of platinum, [Pt], in the colloidal solution is 6.5 mM.

Platinum nanobubbles were prepared by reacting 1.00 mL of the colloidal solution containing SiO_2@Pt core–shell nanospheres with 10.00 mL of 0.5% HF(aq) for 2 min. Then, the products were centrifuged at 10,000 rpm for 10 min and redispersed in 1.00 mL of ethanol three times.

2.3. Characterization of platinum nanocatalysts

Transmission electron microscopic (TEM) images were obtained by a microscope (Carl Zeiss, LIBRA 120), and energy-dispersive X-ray (EDX) line-scanned elemental intensity propfiles and high-resolution TEM (HRTEM) images were measured by using a high-resolution microscope (FEI, Tecnai F20).

The catalytic properties of platinum nanocatalysts were measured by monitoring the reduction reaction of rhodamine B in the presence of KBH_4. 0.40 mL of an ethanol colloidal solution containing platinum nanocatalysts was added into 0.90 mL of water and 1.70 mL of 20 μM rhodamine B(aq) contained in a polyphenyl cell having a path length of 10 mm and then 0.40 mL of 10 mM KBH_4(aq) has been added rapidly. Then, the absorption spectral changes of rhodamine B were measured at scheduled intervals using a temperature-controllable spectrophotometer (Scinco, S-3000).

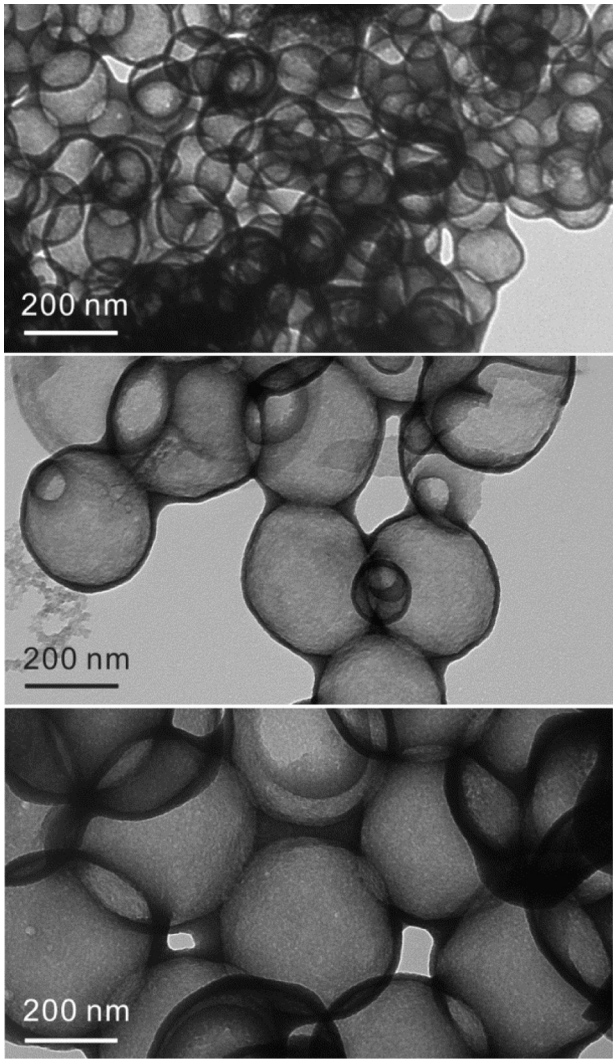

Fig. 2. Transmission electron microscopy (TEM) images of platinum nanobubbles with average diameters of 150 (top), 320 (middle), and 420 nm (bottom).

3. Results and discussion

3.1. TEM images

Fig. 2 shows typical TEM images of platinum nanobubbles having average outer diameters of 150, 320, and 420 nm, illustrating that platinum nanobubbles have empty interiors because the TEM images of individual nanostructures are brighter in the central regions than in the edge regions. The sizes of platinum nanobubbles were controlled by adjusting the template sizes of silica nanospheres, and the sizes of silica nanospheres were adjusted by varying the amounts of 25% NH_3(aq); as the larger volumes of the base were added, the bigger core templates of silica nanospheres were produced.

3.2. EDX line-scanned elemental profiles

The EDX line-scanned elemental profile of platinum measured along the indicated solid line of the platinum nanobubble in the HRTEM image of Fig. 3 exhibits two characteristic sharp peaks very well, indicating that the platinum nanobubble has a very hollow structure evidently. The insetted HRTEM image of Fig. 3 also displays well that the interior of the platinum nanostructure is vacant. The shapes and positions of two peaks of the Pt intensity profile

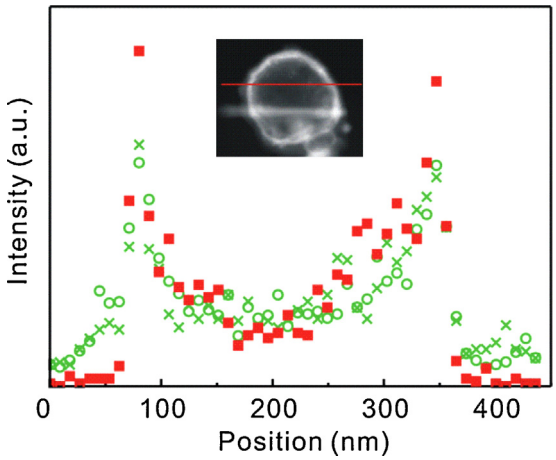

Fig. 3. Area-normalized EDX elemental profiles of a platinum nanobubble scanned along the line in the HRTEM image of the inset. Squares indicate Pt while circles and crosses do Si and O, respectively.

are similar to the respective ones of the Si and the O intensity profiles, indicating that the wall of a platinum nanobubble compositely consists of platinum and silica. However, a close examination of the elemental intensity profiles reveals that the thickness of the platinum shell is 20 nm whereas that of the silica shell is 30 nm. Furthermore, the elemental intensity profiles indicate that silica is also present on the outside of the platinum shell. These suggest that dissolved silica, which were produced during the core etching of SiO_2@Pt core–shell nanospheres with HF(aq), became precipitated again during the washing process to form solid silica, which was in contact with the platinum shell.

3.3. Formation mechanism

As illustrated in Fig. 1, platinum nanobubbles with uniform shell thickness have been prepared by etching the silica cores of SiO_2@Pt core–shell nanospheres. The sol-gel process of TEOS using base catalysts was employed to prepare nearly monodispersive silica nanospheres. Then, the hydroxyl groups on the surfaces of silica nanospheres were treated with APTES to form amino groups on the silica surfaces. We have found that the complete functionalization of the silica surfaces with a sufficient amount of APTES is essential for the proper coating of the silica surfaces with platinum seeds (Fig. S1 in the supporting information). PVP-stabilized platinum seeds with diameters below 5 nm were attached to the surfaces of silica nanospheres. A coordination bond was formed between N and Pt to produce a silica-supported nitrogenous platinum complex (SiO_2–NH_2–Pt), which played an important role in attaching platinum seeds to silica nanospheres [36]. Then, the platinum nanoseeds clustered on silica nanospheres were transformed into platinum shells via the reduction of newly added H_2PtCl_6(aq) with L-ascorbic acid to form SiO_2@Pt core–shell nanospheres. The silica nanocores were excavated completely by reacting the core–shell nanospheres with an excess amount of HF(aq) to produce platinum nanobubbles. HF(aq) has been known to remove silica effectively through the stoichiometric reaction of $SiO_2(s) + 4HF(aq) \rightarrow SiF_4(g) + 2H_2O(\ell)$ [37]. Fig. S2 in the supporting information indicates that 2 min is a sufficiently long reaction time to remove the silica nanocores entirely; the reaction of the core–shell nanospheres with HF(aq) for 30 min has yielded broken platinum nanoshells.

Supplementary material related to this article found, in the online version, at http://dx.doi.org/10.1016/j.apcatb.2013.05.037.

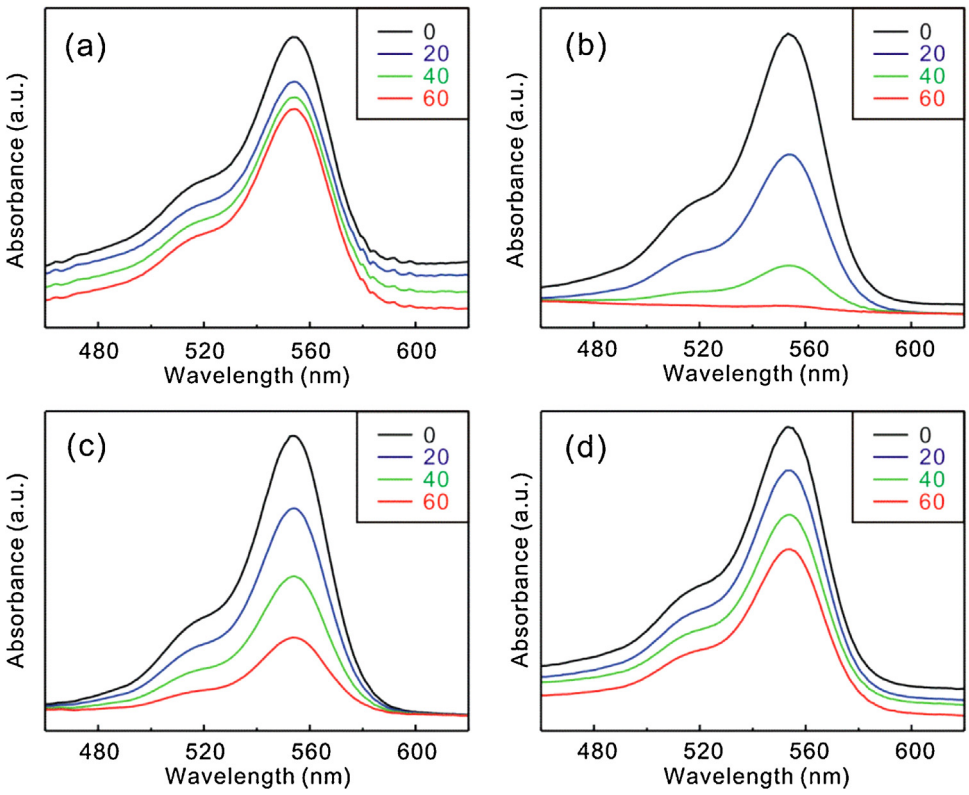

Fig. 4. Absorption spectra at 30 °C of 10 μM rhodamine B solutions in the presence of 1.2 mM KBH_4 after addition of (a) SiO_2@Pt core–shell nanospheres having an average diameter of 150 nm (150 C) and (b) platinum nanobubbles having average outer diameters of 150 nm (150H), (c) 320 nm (320H), and (d) 420 nm (420H), measured at elapsed times indicated in the units of min.

3.4. Catalytic performances

We have explored the catalytic properties of platinum nanobubbles by monitoring time-dependent absorbance changes of rhodamine B degraded catalytically via the nanobubbles in the presence of KBH_4 (Fig. 4). For the sake of comparison, the catalytic performances of SiO_2@Pt core–shell nanospheres have been also measured, revealing that the catalytic performances of platinum nanobubbles are much more efficient than those of SiO_2@Pt core–shell nanospheres at the same concentration. The absorption of rhodamine B decreased much more rapidly in the presence of the nanobubbles (Fig. 4b and c) than in the presence of the core–shell nanospheres (Fig. 4a). Fig. 4b and c displays as well that the catalytic efficiency of platinum nanobubbles increases extensively with the decrease of their sizes (see below).

The temperature-dependent first-order degradation kinetic profiles of rhodamine B via platinum nanocatalysts in the presence of KBH_4 in Fig. 5 have been employed to extract the observed degradation rate constants (k_{obs}); the pseudo-linear plots of $\ln(A/A_o) = -kt$ [38], where A is the optical density at 554 nm of rhodamine B and t is the time of the reaction, yield k_{obs} shown in Table 1. The catalytic rate constant (k_{cat}) of a platinum nanocatalyst can be obtained by subtracting the degradation rate constant (k_0) of rhodamine B in the absence of any nanocatalysts from k_{obs}; $k_{cat} = k_{obs} - k_0$. Note that rhodamine B in the presence of nanocatalysts hardly decomposes in the abscence of KBH_4, suggesting the decolorization of rhodamine B is not due to its adsorption to nanocatalysts [39]. The k_{cat} of 150H, which is larger by 8 times than reported value at 25 °C [39], has been found to be larger by 23 times than that of 150C, suggesting that the excavation of the silica cores of the 150C nanocatalysts enhances the catalytic efficiency enormously. Table 1 also displays that the catalytic efficiency of platinum nanobubbles increases greatly indeed with the decrease

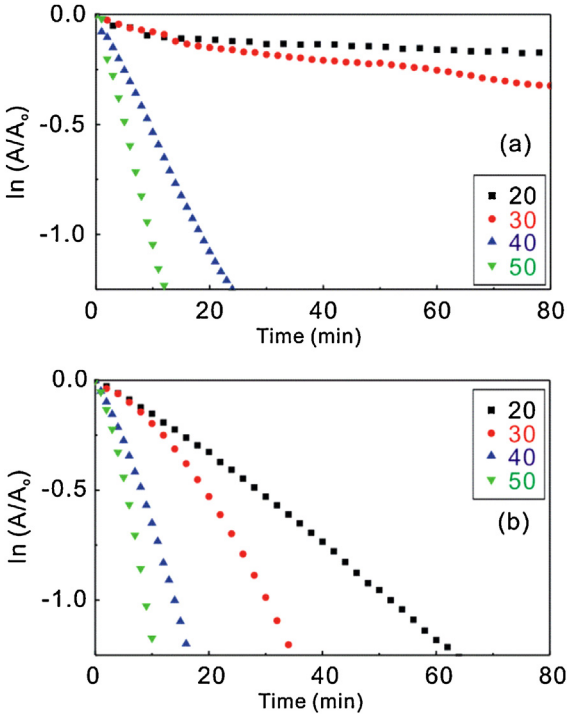

Fig. 5. First-order kinetics, $\ln(A/A_o)$ vs. t, for the catalytic degradation of 10 μM rhodamine B via nanocatalysts of (a) 150 C and (b) 150H in the presence of 1.2 mM KBH_4 at temperatures indicated in the units of °C.

Table 1
Comparison of rate constants, frequency factors, activation energies, and activation entropies for the catalytic degradation of rhodamine B via platinum nanocatalysts in the presence of KBH_4.

Nanoatalyst	k_{obs} at 30 °C (min^{-1})	k_{cat} at 30 °C (min^{-1})	Frequency factor (min^{-1})	Activation energy (kcal mol^{-1})	Entropy of activation (cal mol^{-1} K^{-1})
[a]	0.0028	0			
150C	0.0041	0.0013	3.9×10^{19}	30.5	−14.2
150H	0.032	0.030	1.6×10^{6}	10.7	−29.6
320H	0.021	0.018	3.1×10^{8}	14.5	−17.5
420H	0.0090	0.0062	1.0×10^{9}	15.7	−15.6

[a] In the absence of any nanocatalysts.

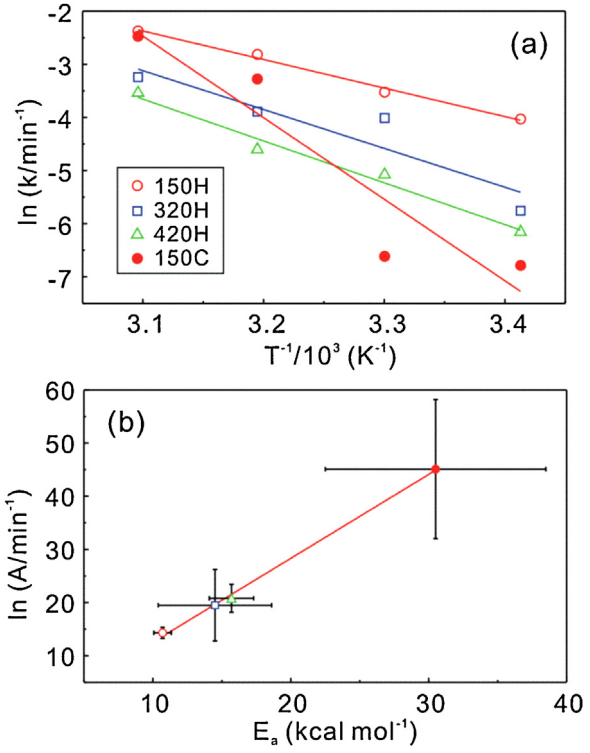

Fig. 6. (a) Arrehenius plots for the catalytic degradation reaction of 10 μM rhodamine B in the presence of 1.2 mM KBH_4 via platinum nanocatalysts indicated inside. (b) The compensation law plot of the activation energies and the frequency factors obtained from the slopes and the intercepts, respectively, of the Arrehenius plots.

of their sizes. The temperature dependence of the kinetic profiles in Fig. 5b is much smaller than that in Fig. 5a, implying that the excavation of 150C reduces the activation energy of k_{cat} substantially (see below).

The frequency factor of the catalytic degradation of rhodamine B via the 150C nanocatalyst extracted from an Arrehenius plot [38] of Fig. 6a is the highest ever reported for this reaction (Table 1) [40,41]. However, the k_{cat} of 150C is rather small due to its large activation energy. The frequency factor and the activation energy of the catalytic degradation via 150H in Table 1 indicate that the excavation of the SiO_2@Pt core–shell nanospheres reduces the activation energy severely and the frequency factor drastically. This then suggests that the catalysis mechanism of platinum nanobubbles is completely different from that of the core–shell nanospheres (see below). Fig. 6a and Table 1 also reveal that both the frequency factor and the activation energy increase gradually with the size increase of platinum nanobubbles. This hints that the catalysis mechanism of platinum nanobubbles remains the same regardless of their sizes within our studied range; the catalytic reaction takes place within the nanocavities of platinum nanobubbles. The decrease of k_{cat}, resulting mainly from the increase of the activation energy, with size increase has been attributed to the reduction of the nanoreactor confinement effect of platinum nanobubbles [41]. Eyring plots [42] have revealed that the entropy of activation for 150H is much larger than that for 150C. Furthermore, the entropy of activation decreases with the size increase of platinum nanobubbles. These also support that the catalytic reaction via platinum nanobubbles takes place within their nanocages whereas the reaction via SiO_2@Pt core–shell nanospheres does on their surfaces.

Fig. 6b shows the existence of a good compensation relation in the catalytic systems of our platinum nanostructures. The following empirical linear relationship has been found to hold between the frequency factor (A) and the activation energy (E_a); $\ln A = \alpha + E_a/(RT_\theta)$ where α is a constant and T_θ is called the fictitious isokinetic temperature, at which the rates on all the nanocatalysts become equal [43,44]. In our systems, T_θ has been found to be 319 K. It is considered that a catalyst such as 150C has a large concentration of active sites where the reaction requires high E_a, while another catalyst such as 150H has a small concentration of active sites that have low E_a for the same catalytic reaction.

Because catalysis by metals is a surface phenomenon, small sizes of nanocatalysts with a large fraction of the atoms exposed to environment have high catalytic properties [45]. The catalytic degradation mechanism of organic pollutants such as rhodamine B in the presence of our platinum nanocatalysts and KBH_4 could be explained as follows. Rhodamine B is electrophilic and BH_4^- is nucleophilic with respect to platinum nanocatalysts. Thus, the nucleophile BH_4^- can donate electrons to platinum nanocatalysts, and the electrophile rhodamine B can capture electrons from the platinum nanocatalysts; platinum nanocatalysts serve as electron relays for the degradation reaction of rhodamine B in an aqueous KBH_4 solution [46]. The catalytic electron relays occur on the outer metallic surfaces of the core–shell nanospheres. However, they take place with much smaller E_a in the nanocavity surfaces of the platinum nanobubbles. Thus, we suggest that the nanoreactor confinement effect of the platinum nanobubble has expedited electron relays from BH_4^- to rhodamine B tremendously by reducing E_a extensively. The size dependence of the catalytic activation energy (E_a) could be obtained from the following relation; $E_a/E_{a,\infty} = T_m/T_{m,\infty} = 1 - \alpha_{shape}/D$ [47]. T_m is the melting temperature of the nanostructure, α_{shape} is the shape parameter defined as $\alpha_{shape} = AD(\gamma_s - \gamma_\ell)(V\Delta H_{m,\infty})$, D is the size of the structure, and A and V are the surface area and volume of the nanostructure, respectively. $\Delta H_{m,\infty}$ is the bulk melting enthalpy and γ_s and γ_ℓ are the surface energy in the liquid and solid phases, respectively. It means that the catalytic activation energy increases with size increase as confirmed with our experimental data in Table 1.

4. Conclusions

Platinum nanobubbles having a uniform shell thickness of 20 nm with average outer diameters of 150, 320, and 420 nm have been successfully prepared by etching the cores of SiO_2@Pt core–shell nanospheres with HF(aq). The sizes of platinum nanobubbles have been controlled by adjusting the template sizes of silica

nanospheres with varying the amount of NH_3(aq). Platinum nanobubbles have been found to catalyze the degradation of organic pollutant dyes such as rhodamine B efficiently in the presence of KBH_4 compared with SiO_2@Pt core–shell nanospheres. We have investigated the catalytic mechanism of the nanocatalysts by monitoring various kinetic parameters such as rate constants, activation energies, frequency factors, and entropies of activation. The temperature dependence of the catalytic degradation rate constants via platinum nanobubbles is much smaller than that via SiO_2@Pt core–shell nanospheres, implying that the catalysis mechanisms of the two different nanocatalysts are completely different. The catalytic activation energy of the degradation of rhodamine B has been found to decrease with the size decrease of platinum nanobubbles. These suggests that the catalytic reaction via platinum nanobubbles occurs within their nanocages, whereas the reaction via SiO_2@Pt core–shell nanospheres does on their surfaces. The existence of a good compensation effect between activation energies and frequency factors has been evidenced for the platinum nanocatalysts, revealing that the isokinetic temperature is 319 K.

Acknowledgments

This work was supported by research grants through the National Research Foundation (NRF) of Korea funded by the Ministry of Education, Science, and Technology (2011-0028981 and 2012-006345). D.J.J. is also thankful to the SRC program of NRF (2007-0056331).

References

[1] J. Lee, S. Mahendra, P.J.J. Alvarez, ACS Nano 4 (2010) 3580–3590.
[2] H. Yoo, J. Sharma, H.-C. Yeh, J.S. Martinez, Chemical Communications 46 (2010) 6813–6815.
[3] Y.H. Kim, J.-Y. Kim, D.-J. Jang, Journal of Physical Chemistry C 116 (2012) 10296–10302.
[4] H.-B. Kim, D.-J. Jang, CrystEngComm 14 (2012) 6946–6951.
[5] J.-Y. Kim, H. Jeong, D.-J. Jang, Journal of Nanoparticle Research 13 (2011) 6699–6706.
[6] S.J. Kim, C.S. Ah, D.-J. Jang, Advanced Materials 19 (2007) 1064–1068.
[7] M.R. Kim, J.-Y. Kim, S.J. Kim, D.-J. Jang, Applied Catalysis A – General 393 (2011) 317–322.
[8] T.K. Sau, A.L. Rogach, F. Jäckel, T.A. Klar, J. Feldmann, Advanced Materials 22 (2010) 1805–1825.
[9] C. Noguez, Journal of Physical Chemistry C 111 (2007) 3806–3819.
[10] S.J. Kim, D.-J. Jang, Materials Letters 62 (2008) 4500–4502.
[11] M.A. Mahmoud, M.A. El-Sayed, Langmuir 28 (2012) 4051–4059.
[12] P.K. Jain, X.H. Huang, I.H. El-Sayed, M.A. El-Sayed, Accounts of Chemical Research 41 (2008) 1578–1586.
[13] J. Gao, X. Ren, D. Chen, F. Tang, J. Ren, Scripta Materialia 57 (2007) 687–690.
[14] H.M. Lu, X.K. Meng, Journal of Physical Chemistry C 114 (2010) 1534–1538.
[15] H. Ataee-Esfahani, Y. Nemoto, L. Wang, Y. Yamauchi, Chemical Communications 47 (2011) 3885–3887.
[16] L. Kuai, S. Wang, B. Geng, Chemical Communications 47 (2011) 6093–6095.
[17] J. Wang, Z. Jiang, Z. Zhang, Y.P. Xie, X.F. Wang, Z.Q. Xing, R. Xu, X.D. Zhang, Ultrasonics Sonochemistry 15 (2008) 768–774.
[18] Q. Tang, X. Huang, Y. Chen, T. Liu, Y. Yang, Journal of Molecular Catalysis A: Chemical 301 (2009) 24–30.
[19] P. Huber, B. Carré, Bioresources 7 (2012) 1366–1382.
[20] R. Narayanan, M.A. El-Sayed, Nano Letters 4 (2004) 1343–1348.
[21] Y. Li, J. Petroski, M.A. El-Sayed, Journal of Physical Chemistry B 104 (2000) 10956–10959.
[22] T. Herricks, J. Chen, Y. Xia, Nano Letters 4 (2004) 2367–2371.
[23] R. Krishnaswamy, H. Remita, M. Inpéror-Clerc, C. Even, P. Cavidson, B. Pansu, ChemPhysChem 7 (2006) 1510–1513.
[24] Y.-J. Han, J.M. Kim, G.D. Stucky, Chemistry of Materials 12 (2000) 2068–2069.
[25] Y. Luo, S.K. Lee, H. Hofmeister, M. Steinhart, U. Gösele, Nano Letters 4 (2004) 143–147.
[26] Y. Song, Y. Yang, C.J. Medforth, E. Pereira, A.K. Singh, H. Xu, Y. Jiang, C.J. Brinker, F.V. Swol, J.A. Shelnutt, Journal of the American Chemical Society 126 (2004) 635–645.
[27] H. Wang, Y. Song, C.J. Medforth, J.A. Shelnutt, Journal of the American Chemical Society 128 (2006) 9284–9285.
[28] M.R. Kim, D.K. Lee, D.-J. Jang, Applied Catalysis B: Environmental 103 (2011) 253–260.
[29] X.W. Lou, L.A. Archer, Z. Yang, Advanced Materials 20 (2008) 3987–4019.
[30] Y. Yin, R.M. Rioux, C.K. Erdonmez, S. Hughes, G.A. Somorjai, A.P. Alivisatos, Science 304 (2004) 711–714.
[31] H.G. Yang, H.C. Zeng, Journal of Physical Chemistry B 108 (2004) 3492–3495.
[32] F. Caruso, Chemistry – A European Journal 6 (2000) 413–419.
[33] W. Stöber, A. Fink, E. Bohn, Journal of Colloid and Interface Science 26 (1968) 62–69.
[34] J.W. Kim, L.U. Kim, C.K. Kim, Biomacromolecules 8 (2007) 215–222.
[35] V.R. Calderone, J. Schütz-Widoniak, G.L. Bezemer, G. Bakker, C. Steurs, A.P. Philipse, Catalysis Letters 137 (2010) 132–140.
[36] J. Li, C. Yang, L. Zhang, T. Ma, Journal of Organometallic Chemistry 696 (2011) 1845–1849.
[37] B. Liu, W. Zhang, H. Feng, X. Yang, Chemical Communications 47 (2011) 11727–11729.
[38] N.S. Langeroodi, Russian Journal of Physical Chemistry A 86 (2012) 628–631.
[39] M.A. Mahmoud, M.A. El-Sayed, Nano Letters 11 (2011) 946–953.
[40] J. Zeng, Q. Zhang, J. Chen, Y. Xia, Nano Letters 10 (2010) 30–35.
[41] M.A. Mahmoud, F. Saira, M.A. El-Sayed, Nano Letters 20 (2010) 3764–3769.
[42] K.D. Zimmer, R. Shoemaker, R.R. Ruminski, Inorganica Chimica Acta 359 (2006) 1478–1484.
[43] T. Bligaard, K. Honkala, A. Logadottir, J.K. Norskov, S. Dahl, C.J.H. Jacobsen, Journal of Physical Chemistry B 107 (2003) 9325–9331.
[44] G.A. Somorjai, Introduction to Surface Chemistry and Catalysis, John Wiley & Sons Inc., USA, 1994.
[45] Z. Xu, F.-S. Xiao, S.K. Purnell, O. Alexeev, S. Kawi, S.E. Deutsch, B.C. Gates, Nature 372 (1994) 346–348.
[46] Z. Deng, M. Chen, L. Wu, Journal of Physical Chemistry C 111 (2007) 11692–11698.
[47] G. Guisbiers, G. Abudukelimu, D. Hourlier, Nanoscale Research Letters 6 (2011) 396(1)–396(5).